Forensic volumetric visualization of gunshot residue in its anatomic context in forensic post mortem computed tomography: Development of transfer function preset

Schweitzer, Wolf ; Verster, Janette ; Aldomar, Eloisa ; Ebert, Lars ; Bolliger, Stephan A ; Thali, Michael J ; Ampanozi, Garyfalia

Abstract: While the visualization of gunshot injuries so far focused on solid metal density in routine forensic post mortem computed tomography (PMCT) as well as in micro-computed tomography, gunshot residue (GSR) as dispersed metal particles typically succumbs to partial volume effect. A case series of seven contact shots to the head was evaluated to determine a density range for GSR with at least three times higher likelihood than encountering bone, skin, muscle or blood. For that, a Bayesian likelihood was determined from normal distributions of the CT-densities of blood, bone, skin, muscle and GSR as identified in correlation with visual evidence. Resulting transfer functions matched ring and cone shaped GSR deposits as published elsewhere, thus representing a plausible result. Only fast and plausibly specific visualization is suitable for routine use in forensic PMCT, to allow the examination of GSR in real cases on a wider scale.

DOI: https://doi.org/10.1016/j.fri.2021.200451

Posted at the Zurich Open Repository and Archive, University of Zurich
ZORA URL: https://doi.org/10.5167/uzh-205153
Journal Article
Published Version

Originally published at:
Schweitzer, Wolf; Verster, Janette; Aldomar, Eloisa; Ebert, Lars; Bolliger, Stephan A; Thali, Michael J; Ampanozi, Garyfalia (2021). Forensic volumetric visualization of gunshot residue in its anatomic context in forensic post mortem computed tomography: Development of transfer function preset. Forensic Imaging, 25:200451.
DOI: https://doi.org/10.1016/j.fri.2021.200451

Forensic Imaging 25 (2021) 200451

Contents lists available at ScienceDirect

Forensic Imaging

journal homepage: www.sciencedirect.com/journal/forensic-imaging

Forensic volumetric visualization of gunshot residue in its anatomic context in forensic post mortem computed tomography: Development of transfer function preset

Wolf Schweitzer [*,a], Janette Verster [a,b], Eloisa Aldomar [c], Lars Ebert [a], Stephan A. Bolliger [a], Michael J. Thali [a], Garyfalia Ampanozi [a]

[a] Department of Forensic Medicine and Imaging, Zurich Institute of Forensic Medicine, University of Zurich, Switzerland
[b] Division of Forensic Medicine, Faculty of Health Sciences, Stellenbosch University, Stellenbosch, South Africa
[c] Knowledge Visualization, Department of Design, ZHdK Zurich University of the Arts, Zurich, Switzerland

ARTICLE INFO

Keywords:
Virtopsy
post mortem computed tomography
forensic visualization
gunshot
gunshot residue

ABSTRACT

While the visualization of gunshot injuries so far focused on solid metal density in routine forensic post mortem computed tomography (PMCT) as well as in micro-computed tomography, gunshot residue (GSR) as dispersed metal particles typically succumbs to partial volume effect. A case series of seven contact shots to the head was evaluated to determine a density range for GSR with at least three times higher likelihood than encountering bone, skin, muscle or blood. For that, a Bayesian likelihood was determined from normal distributions of the CT-densities of blood, bone, skin, muscle and GSR as identified in correlation with visual evidence. Resulting transfer functions matched ring and cone shaped GSR deposits as published elsewhere, thus representing a plausible result. Only fast and plausibly specific visualization is suitable for routine use in forensic PMCT, to allow the examination of GSR in real cases on a wider scale.

Background

Since the first threedimensional visualization of gunshot residue (GSR) in contact shots and close range shots in routine computed tomography (CT) scans [1], visualization methods have made considerable progress [2,3]. In that first paper [1], GSR was described to be visible in a routine CT scanner within a CT-density range of 150 to 3017 Hounsfield units (HU). The observed patterns contained rings, cone-shaped clusters and amorphous scattering of material in proximity to the entrance wound and associated bullet track.

Ideally, a specific, rapid visualization is desirable to allow further investigation of presumed GSR distribution and content. It currently is considered a software standard across various modern volume rendering technique (VRT) programs that CT density display parameters can be edited by the user. There, a transfer function describes the way CT data is encoded in color and opacity values. A transfer function there is implemented easiest by creating a software preset that encodes the required transfer function (see Fig. 1).

In this technical note, a CT-density based approach to test the feasibility of a specific gunshot residue visualization and application in a case series of post mortem computed tomography (PMCT) data is described.

Methods and material

After editing the transfer functions to enable GSR visualization generally (Fig. 1), definitive CT-density values for this method were established based on statistical assessment across all seven cases; thereby, measurements taken from axial slices (see slice image morphologies in Fig. 2) were used for a statistical model (Fig. 3).

PMCT data

A dual source / energy CT scanner (Somatom Definition Flash, Siemens Healthineer Headquarters, Erlangen, Germany) was used (120 kVp tube voltage, maximal data collection diameter 500 mm, collimation 0.6 mm, automatic dose modulation). PMCT data was scanned using pre-defined protocols [4]. Reconstruction image dimensions were taken from the embedded scale on 3D-visualization and used for scale bars.

* Corresponding author.
E-mail address: wolf.schweitzer@irm.uzh.ch (W. Schweitzer).

https://doi.org/10.1016/j.fri.2021.200451
Received 6 January 2021; Accepted 2 April 2021
Available online 24 April 2021

Case series

A series of seven cases with suicidal head shots was used for the development and visualization of presumed GSR.

Two cases (1 and 2) are shown in direct correlation between the transfer function diagram and the 3D-visualization output (Fig. 1).

Case 1 (Fig. 1 7–10): 55 year old man, pistol Jennings, calibre.22. Left temple with triangular skin substance defect and tear towards the ear. Underlying round skull substance defect with associated burst fractures. Postmortem decomposition with an estimated post-mortem interval of about five days. Individual PMCT details: reconstruction kernel H31s[1], reconstruction diameter[2] 267 mm, pixel spacing[3] 0.52 mm, image distance[4]0.4 mm. Time of last CT calibration within 1 hour of PMCT.

Case 2 (Fig. 1 11–14): 74 year old man, pistol Walther PPK 765. Partly skeletonized body, skin defect at right temple, underlying bone defect fracture with radiating burst fracture lines. Individual PMCT details: reconstruction kernel H31s, reconstruction diameter 243 mm, pixel spacing 0.47 mm, image distance 0.4 mm. Time of last CT calibration within 1 hour of PMCT.

Case 3 (Fig 4): 70 year old man, revolver Taurus model 85S, calibre.38 special. – Star-shaped skin tear wound around entrance wound at the right temple. Substance defect, wound edges squashed, with round defect of skull underneath. Black material consistent with GSR is visible in circular arrangement around wound on skin as well as in deeper layers under the entrance wound. The available photograph is from the death scene and contains blood and hair covering the skin wound. PMCT shows an oval thin centrally empty attenuation increase at the skin wound, typical in shape, attenuation and location for GSR. There is the skull defect underneath the skin defect, with fragments in place and a number of centrifugal burst fracture lines. – The exit wound on the left temple, about 5 cm above the left ear, was a 2 x 1,5 cm sized skin perforation with star shaped tears but no substance defect after skin margin adaptation. The skin and underlying bone injury did not show dark material, thus lacking visual indication of GSR. – Individual PMCT-details: reconstruction kernel H31s, reconstruction diameter 256 mm, pixel spacing 0.5 mm, image distance 0.4 mm. Time of last CT calibration within 1 hour of PMCT.

Case 4 (Fig. 5): 77 year old man found dead with what then was

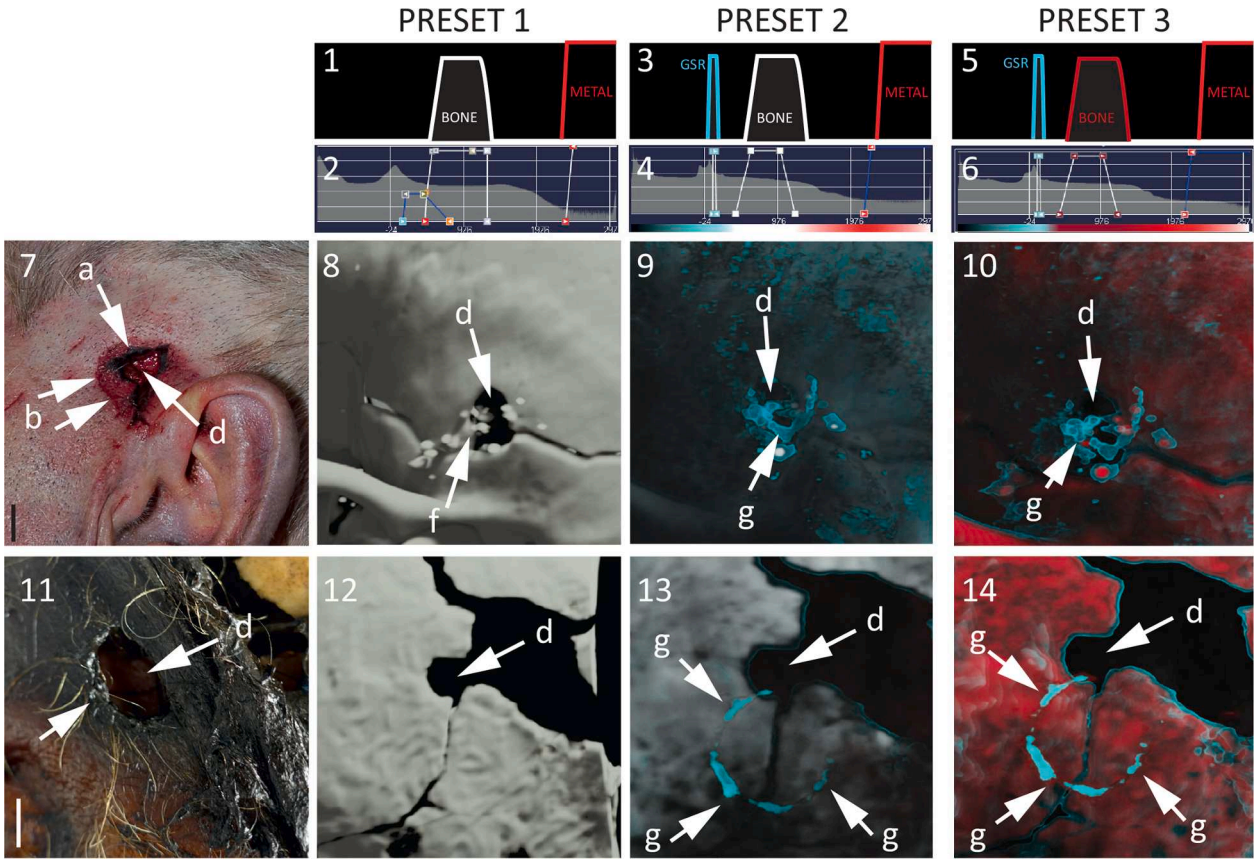

Fig. 1. Transfer functions and 3D reconstructions in comparison – This image shows two cases (case 1: images 7–10; case 2: images 11–14), whereas the reader may compare matching photos (7, 11) and 3D-visualisations of PMCT data using conventional transfer functions for skeletal structures ('preset 1' as shown in 1, 2, 8, 12) as well as new transfer functions ('preset 2' as shown in 3, 4, 9, 13; 'preset 3' as shown in 5, 6, 10, 14) vice versa a technical diagram highlighting details of these transfer functions ('preset 1': 1, 2; 'preset 2': 3, 4'; 'preset 3': 5, 6). Whereas a conventional transfer function ('preset 1') may highlight bone (1: white ramp) and visually set this off against material of a typical metallic density (1: red ramp), scattered GSR material appears to be more likely to occur in relatively lower density ranges (see also Fig. 2), mainly due to partial volume effect. Using what we estimated to be a GSR-typical CT-density in new transfer functions with relatively sharp delineation as a relatively intransparent color ramp (3,5: cyan ramp, relatively high opacity) causes new shapes to appear in the 3D-visualisation (9–10, 13–14) that were not visible with similar clarity beforehand. There, soft tissues immediately overlying the gunshot injuries appear to reveal GSR-typical configurations (9, 10: arrows) not only relatively shortly after death, but a suspected entrance wound may show circular deposits of GSR-typical density even after decomposition has set in (13, 14: arrows). – Case 1: suicidal contact head shot, leaded ammunition, Jennings 22 caliber pistol. Case 2: decomposition with estimated post-mortem interval of about five days, Walther PPK 765 pistol, headshot with entrance at right temple, exit at left temple; findings were deemed to be consistent with suicide. – Bar ~1 cm.

[1] tag 0018,1210
[2] tag 0018,1100
[3] tag 0028,0030
[4] difference between adjacent coordinates tagged 0018,9318

interpreted as fatal headshot next to a Swiss army pistol (SIG Sauer P 226). Entrance wound at right temple with a central skin defect and two discernible tears, towards the caudal direction the abraded rim extends into a patterned abrasion, matching the pistol's front structures relatively well. The rim of the skin wound visually shows grayish dark discoloration, consistent with the assumption of GSR there. The exit wound at the left side of the head, through the parietal bone, shows a lacerated wound from which brain tissue and blood appears to extend. Individual PMCT details: reconstruction kernel H31s, reconstruction diameter 273 mm, pixel spacing 0.53 mm, image distance 0.4 mm. Time of last CT calibration ~7 h before PMCT.

Case 5 (Fig. 6): 74 year old man, pistol Glock (9 mm). – Entrance wound: gaping wound at right temple with star shaped tears, dark material up to 3 mm width that is lining the wound can be seen. The skull contains a defect fracture with radiating burst fracture lines. – At the exit wound on the parieto-occipital right side, the skin shows a star shaped tear with a central defect. The exit wound was also visualized to illustrate a possible role of checking for GSR, with a negative result, when trying to discriminate between entrance and exit wound. Individual PMCT details: reconstruction kernel H31s, reconstruction diameter 254 mm, pixel spacing 0.49 mm, image distance 0.4 mm. Time of last CT calibration within 1 hour of PMCT.

Case 6 (Fig. 7): 62 year old man, pistol Glock 17, caliber 9 x 19. Right temple with penetrating skin defect of around 2 cm diameter. Wound

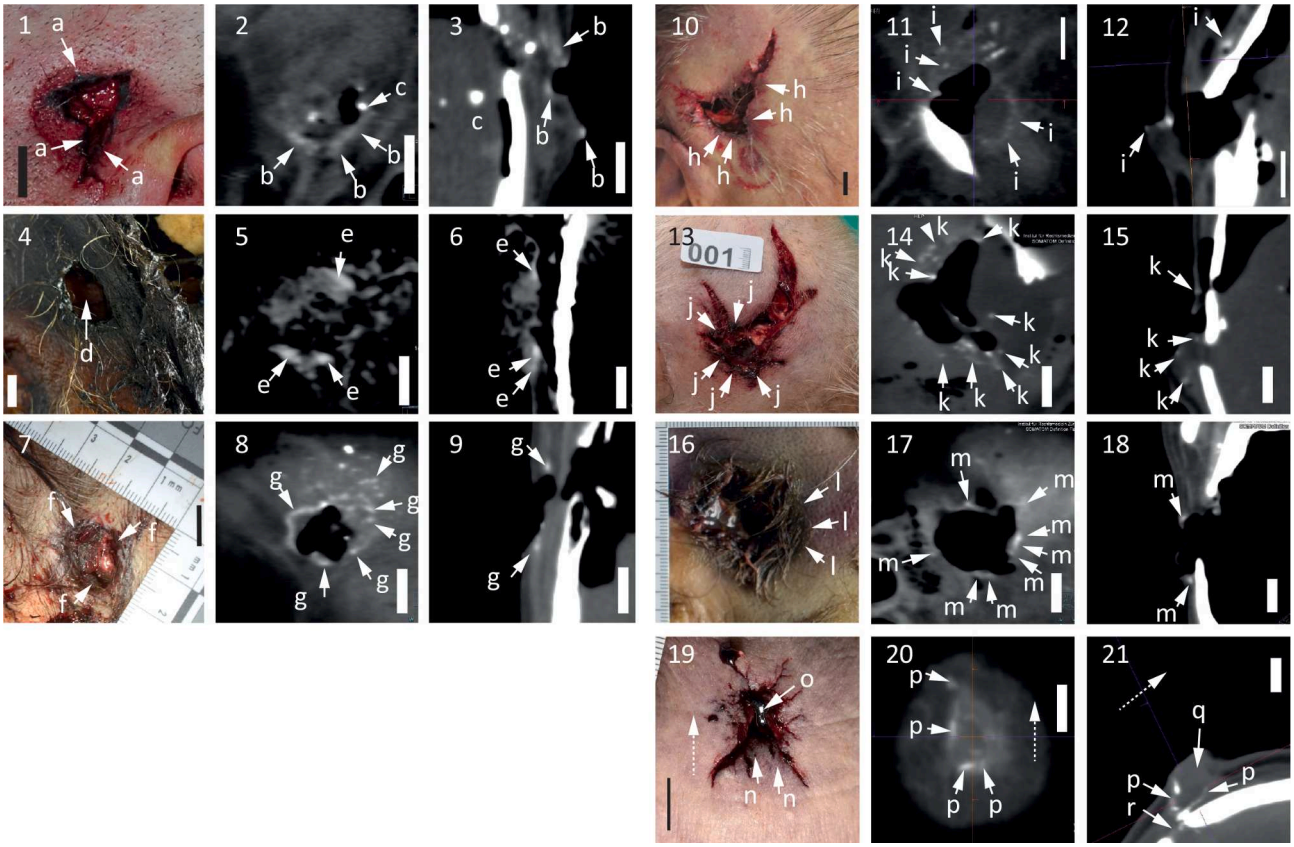

Fig. 2. Conventional PMCT appearance of what assumedly is GSR – Photos of headshot entrance wounds of all seven cases (case 1: images 1–3; case 2: images 4–6; case 3: images 7–9; case 4: images 10–12; case 5: images 13–15; case 6: images: 16–18; case 7: 19–21), in correlation with a multiplanar image placed orthogonally to assumed shot direction through the entrance wound's soft tissues (images 2, 5, 8, 11, 14, 17, 20), and another respective image reconstructed alongside each assumed shot direction (images 3, 6, 9, 12, 15, 18, 21). As described in the first paper about GSR in PMCT, [1], rings, cone-shaped clusters and amorphous scattering of material in proximity to the entrance wound and associated bullet track were sought. – Case 1 (images 1–3) shows darkening of wound edges visually suggestive of GSR (a) with a somewhat triangular lacerated wound and rounded abrasion typical for a contact shot. PMCT with in part ring shaped, in part scattered blurred CT-dense deposits (b) in the immediate surrounding of the skin and bone defect, whereby bone fragments seem to appear considerably less blurred and contain higher CT-density (c). – Case 2 (images 4–6) shows skin defect of entrance wound (d) but no discernible discoloration indicative of possible GSR; PMCT shows blurred softly enhanced CT-density with a ring shape (e) directly under and around the skin defect. – Case 3 (images 7–9) visually exhibits a somewhat oval skin defect with grayish discoloration along its margins (f), whereas PMCT surrounding that skin defect appears to be both somewhat circular and scattered (g), while bone fragments (not labelled, images 8 and 9) seem easy to discern from that appearance due to higher density. – Case 4 (images 10–12) shows an entrance skin wound with both perforation and tears / lacerations, with patterned abrasions typical for a contact shot, whereby the wound margins appeared to exhibit a grayish discoloration (h); the patterned abrasion slightly caudally, adjacent to the entrance wound, appeamatched the shape and size of the pistol's front structures. At that location directly surrounding the wound defect, blurred scattered CT-dense deposits were seen, in part arranged in a ring-shaped or circular fashion (i). – Case 5 (images 13–15) has what appears to be a central skin defect injury with several centrifugal tears, whereas the skin close to the defect exhibits a grayish discoloration consistent with the assumption of GSR (j). PMCT at that location exhibits blurred scattered CT-dense deposits around the wound (k) – Case 6 (images 16–18) show a headshot with a rounded entrance defect wound, that has dark discoloration at its margin (l); PMCT shows blurred CT-dense deposits around the wound in scattered configurations (m). – Case 7 (images 19–21) with a defect wound on the forehead (dashed arrow indicated direction from front to back to allow for better orientation); the skin defect appears to be central, with centrifugal tears, whereas the margin (n) and the blood at the wound (o) both showed a somewhat reflective gray scattered discoloration, a reflection of the light of almost metallic quality. The blood drop (q) that was still in place when the PMCT was scanned indeed showed CT-dense material (p) that was blurred, slightly CT-dense, but appeared shifted in relation to the skull defect (r), consistent with the assumption that the ring shaped scattered deposits (image 20, p) were in part displaced by the blood that had emerged from the wound and then coagulated as a large drop in place (q). – Bar ~1 cm; PCMT windowing with width at ~ 250-300 and centre at ~110 Hounsfield units.

margins with dark discolouration. Underlying skull bone with oval defect and associated burst fracture lines. Individual PMCT details: reconstruction kernel H31s, reconstruction diameter 245 mm, pixel spacing 0.48 mm, image distance 0.4 mm. Time of last CT calibration within 1 hour of PMCT.

Case 7 (Fig. 8): 51 year old man, pistol Beretta 950 B, calibre 6.35. Entrance wound on forehead with attached dried up coagulated blood with the clot measuring around 5 x 10 mm; underneath, star shaped tear wound with central substance defect. The wound margin appears dark. Underneath, there is a round frontal skull bone defect. Individual PMCT details: reconstruction kernel H31s, reconstruction diameter 282 mm, pixel spacing 0.55 mm, image distance 0.4 mm. Time of last CT calibration within 1 hour of PMCT.

Gunshot residue (GSR): characterization and statistics

Written reports and photographs were used to narrow localization of presumed GSR. For the identification of tissue and presumedly GSR-specific CT-densities, visually matched regions of interest (ROI) were measured on axial slices by performing manual ROI-placement. Blood, muscle, bone and epidermal skin were measured using similarly manually placed ROIs into known regions without apparent pathology or trauma. To account for partial volume effect of bone fragments, only relatively small fragments of about 2 mm size were measured. For model definition, six cases were used; for illustration, a seventh case was added. Density averages and standard deviations resulted that were then used to develop the transfer functions (see Results).

editing and all 3D-visualization was initially performed in a commercial product (syngo.via[5]), and for the illustrations in this paper, the transfer functions were transferred to a free software that was used for 3D-visualization, MeVisLab[6]; the pipeline used there was DirectDicomImport > ApplyDicomPixelModifiers > SoPathTracerVolume > SoExaminerViewer combined with SoPathTracerAreaLight; SoPathTracerBackgroundLight; SoPathTracerMaterial [principled]; SuLUTEditor; SoPathTracer [render mode: path tracing; 3000 iterations] > SoExaminerViewer.

Technical development and results

Transfer function basis and definition

CT-density values d were measured manually in regions of interest based on conventional CT slice images (as in Fig. 2), resulting in an average and standard deviation for four different tissues (t), skeletal muscle (s), blood (b), epidermal skin (e) and bone (n) (there, fragments of ~ 2 mm diameter were measured to account for partial volume effect) as well as description and photo matched areas for assumed GSR (g), thus obtaining $\mu_{d^t} \pm \sigma_{d^t}$ with $t \in (g, s, b, e, n)$. With that, we focused our function on the tissues that we esteemed to contain parameters of main visual impact, while not taking extra parameters with suspected less impact into account [5]. This will become apparent when considering what other tissues will still tend to get highlighted with such a visualization.

Fat was not considered for inclusion in this model, as its density

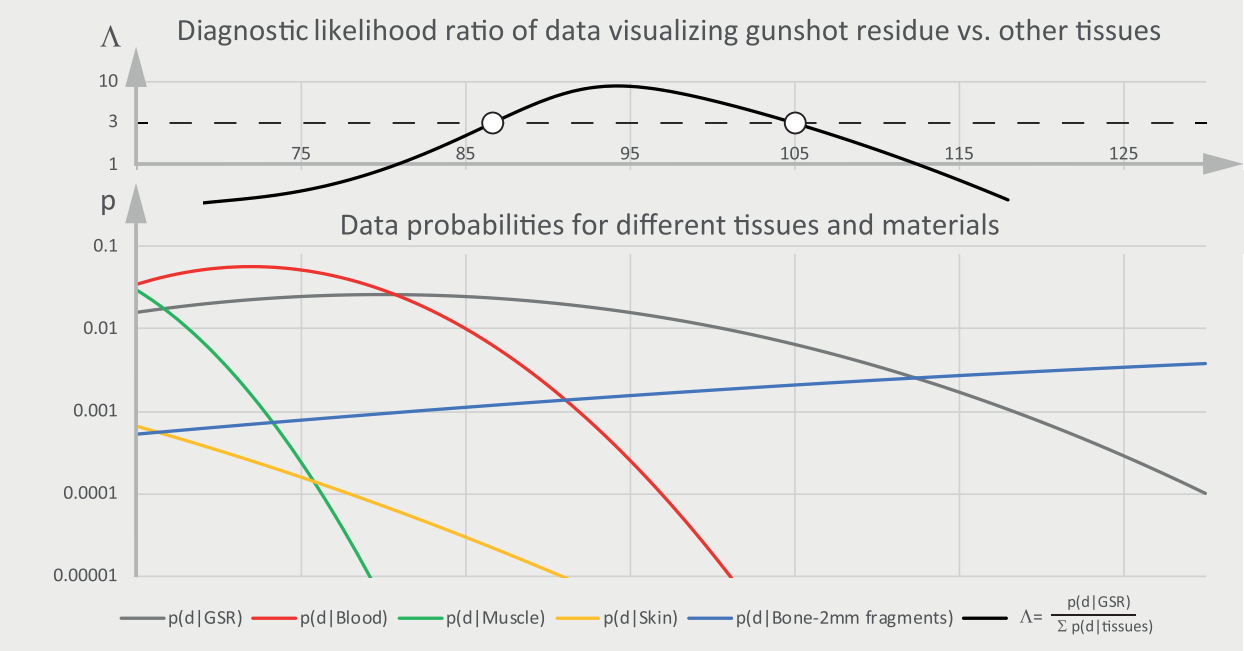

Fig. 3. Statistical model – The chance of diagnostically encountering presumed GSR can be estimated from considering the CT-densities of various tissues and materials. Thereby, the chance to encounter a particular tissue, considering all other tissues present in the visualized data volume, can be calculated as function of CT-density. This diagram shows the normal distribution for the mean CT-density and their standard deviations obtained across five materials of six cases. The resulting likelihood ratio to encounter presumed GSR in comparison has been determined (top), where a threshold of 3 was marked in the diagram with a horizontal line, whose intersection with the likelihood ratio curve yields a density range of 87 to 105 HU to represent presumed GSR with at least three times higher likelihood than representing other tissues that were considered. Please note that some other tissues were not considered for practical reasons. - x-Axis: CT-densities in Hounsfield units [HU]; y-axis: relative data probabilities / likelihood ratio (logarithmic).

Software

Statistics to establish the statistical model based on CT density measurements (see also Fig. 2) was performed using Microsoft Excel (Microsoft, Redmond, California, United States). Transfer function

[5] Siemens Healthineers Headquarters, Erlangen, Germany
[6] MeVis Medical Solutions AG, Fraunhofer Institute for Digital Medicine, MEVIS, Bremen, Germany

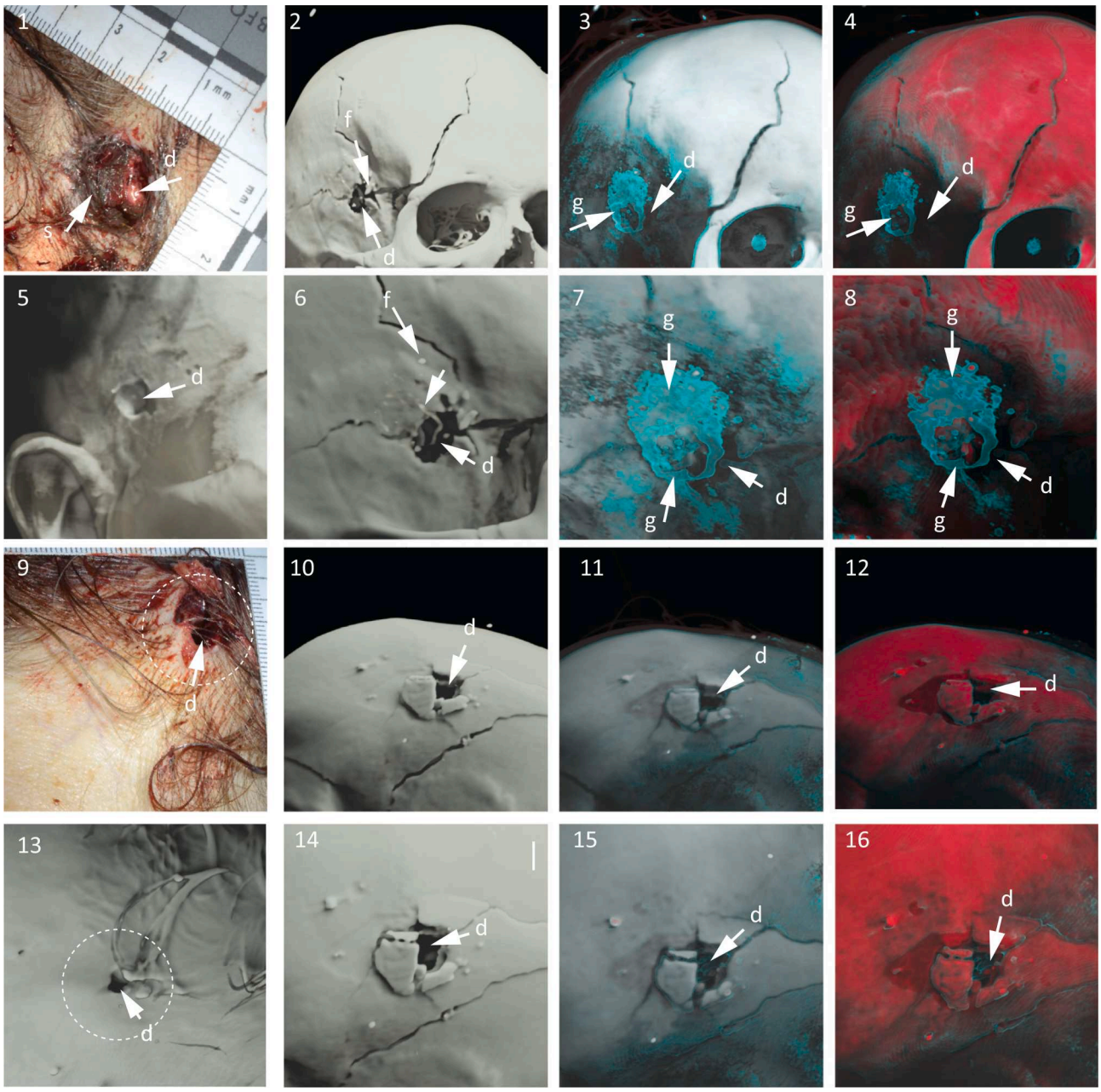

Fig. 4. Case 3 – Entrance wound (1–8): on external inspection, the margin of the defect (1 and 5: d) of the entrance wound showed black material consistent with GSR in circular arrangement around wound on skin (1: s) as well as in deeper layers under the entrance wound after a presumed contact shot. Conventional skeletal PMCT (2, 6) shows the defect (d) and fracture lines f). New transfer functions (3, 4, 7, 8) show a correlate for presumed GSR: it appears to be a perforated flat structure (2, 3, 5, 6: arrows) of about 20 mm diameter. The exit wound (9–16) showed no such large configuration of what we regarded as GSR-typical appearance. PMCT without GSR enhancement shows bone injuries (2, 6, 10, 14) well but presence or absence of presumed GSR remains visually elusive. – Comparison of presets (2, 6, 10, 14: preset 1; 3, 7, 11, 15: preset 2; 4, 8, 12, 16: preset 3) appears to show good contrast of GSR with preset 3. – Bar ~1 cm.

(usually around -10 HU) is so low that it is outside the range of densities considered for this visualization. Also, typical solid metal densities were not considered as they were considered to be too high to practically impact this visualization. Cartilage and ocular lenses were not considered as they were assumed to not interfere with the visual search for presumed GSR considering the typical or most often encountered anatomical distribution of injuries and particles related to head shots [6]. Considerable overlap of CT-densities of presumed GSR with these of cartilage or periost appeared to make presumed GSR visualization difficult if not impossible, so a technical concession was made by not including cartilage and periosteal tissue in the model. Also this visualization was primarily targeted for soft tissues such as cutaneous and subcutaneous structures.

Then, the probabilities of encountering a particular density d as belonging to a particular tissue t, assuming normal distribution, were approximated across a CT-density range of $d \in [\![65, 130]\!]$ (bottom diagram in Fig. 2):

$$p(d|t) = f(\mu_{d^t}, \sigma_{d^t}); d \in [\![65, 130]\!]; t \in (s, b, e, n, g) \quad (1)$$

From these, a Bayesian likelihood ratio to encounter a data value belonging to presumed GSR g in context of the four other tissues was approximated (top diagram in Fig, 2) in approach similar to previously published 3D-visualization classification [7]:

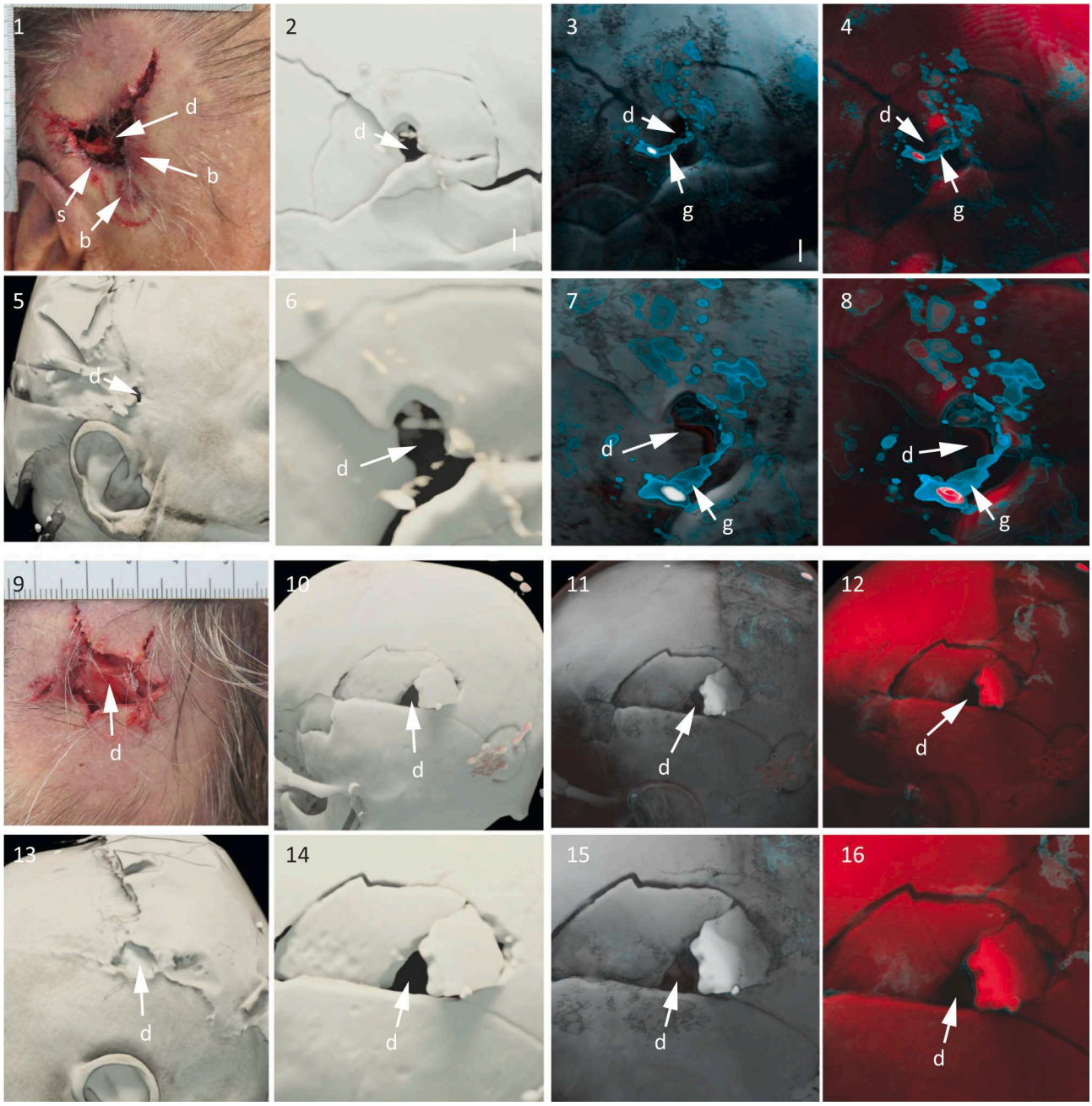

Fig. 5. Case 4 – This entrance wound (1–8) – as a contact wound – appears to show a skin defect (d) with adjacent weapon face derived abrasions at caudal margin of skin perforation (1: b) and GSR typical dark discoloration around the wound edges (1: s) and on the skin extending caudally. GSR-typical value range reconstructions (3, 4, 7, 8) shows a ring-shaped structure (g), consistent with the assumption of GSR in the vicinity of the bony entrance defect (d). The exit wound (9–16) shows no such structure indicative of possible GSR close to bony defect (d). – Comparison of presets (2, 6, 10, 14: preset 1; 3, 7, 11, 15: preset 2; 4, 8, 12, 16: preset 3) appears to show good contrast of GSR with preset 3. – Bar ~1 cm.

$$\Lambda\left(\frac{d|g}{d|s\cup b\cup e\cup n}\right)=\frac{p(d|g)}{\sum_{x\in(s,b,e,n)}p(d|x)} \tag{2}$$

An arbitrary threshold of $\Lambda \geq 3$ was used to identify the CT-density range to attribute to presumed GSR for visualization with reasonable likelihood. With that, CT-densities were likely to visually stand out as possible GSR from the the selected other tissues with an at least threefold likelihood, when separately highlighted within a CT-density range of 87 to 105 HU, based on our six cases. As the case details show, soft kernel reconstructions were used.

Based on these assessments and assumptions, the visualization thus was geared to highlight CT-densities that are at least three times more likely to belong to presumed GSR rather than the other tissues that had been considered.

The implementation of the transfer function provides one density ramp of high but not complete opacity for the density range identified as more likely to represent presumed GSR (87 to 105 HU) than the other tissues. Arbitrarily, cyan was chosen as color for that. When comparing suitable colors for the visual background that usually is bone in head shots, a white color (Fig. 1, preset 2) and a red color (contrasting the cyan of GSR better, preset 3) were compared also against a conventional preset (Fig. 1, preset 1). The remainder of the transfer function options were manually optimized for shadow, depth and reflection.

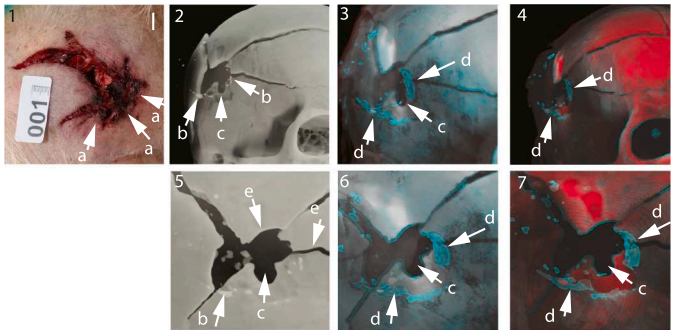

Fig. 6. Case 5 – The entrance wound with star shaped tears contains dark discolouration particularly at the fronto-caudal wound margins (1: a). At that same location, circumferential GSR-typical enhancement becomes visible in 3D-visualization (d), while relative position and extent or size can be appreciated in context of bone injury (c: roundish perforating defect; e: other fracture bone edges). – Comparison of presets (2, 5: preset 1; 3, 6: preset 2; 4, 7: preset 3) shows good contrast of GSR with preset 3. – Bar ~1 cm.

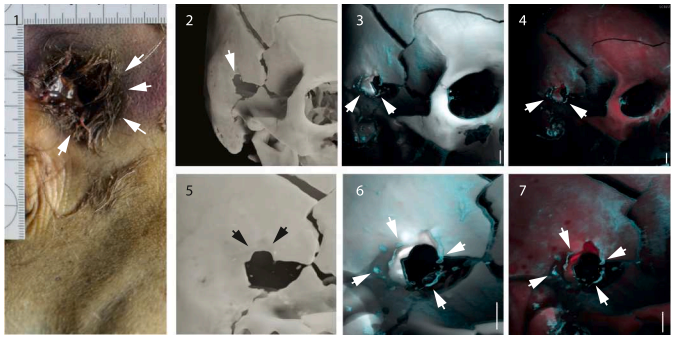

Fig. 7. Case 6 – The extent and location of the dark discoloration around the wound when inspected (1: arrows) appears to roughly correlate with a thin, circumferential GSR-typical enhancement on 3D-visualization (3, 4, 6, 7: arrows). The appearance is that of a subtle ring. – Comparison of presets (4, 7: preset 3; 3, 6: preset 2; 2, 5: preset 1) shows best contrast of GSR with preset 3. – Bar ~1 cm.

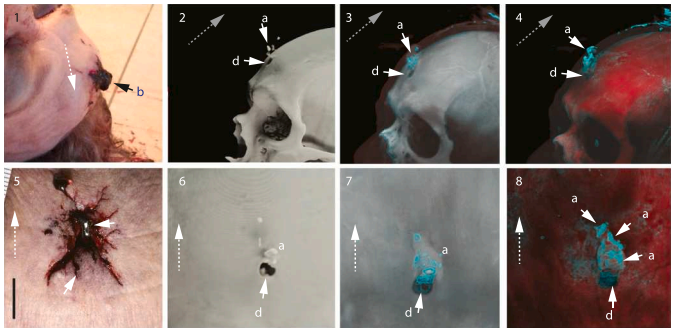

Fig. 8. Case 7 – The entrance defect with star shaped tears also contains a significant blood clot (1: black arrow, label b; 5: top white arrow) (dashed white arrow pointing from front to back for orientation across images 1-8). Upon direct inspection, the blood clot appeared to reflect light differently than when just containing blood and a partial GSR content was assumed already at that stage. As that question was assumed to be of possible reconstructive interest, it was left in place for PMCT. There, the whole blood clot appears to stand out visually exhibiting increased CT-density (2, 6: arrows). This shows that GSR as material may undergo further dynamic configuration change as part of ante- or peri-mortal processes such as hemorrhage. The conventional bone reconstruction (4, 8) does not fully capture these details (compare 6, 7 and 8). – Comparison of presets (4, 8: preset 1; 3, 7: preset 2; 2, 6: preset 3) shows best contrast of GSR with preset 3. – Bar ~1 cm.

Visualization results

The visualization results using three presets (Fig. 1) are shown in detail in Figures 3, 4, 5, 6, 7, 8 and summarized in Table 1.

Overall, best visualization of GSR resulted with a contrasting background color. The application of the presets within the software used was usually achieved in a few seconds (user interface activities: opening window to change preset, changing preset, confirming choice).

In all cases, clearly false positive GSR-typical densities were visible in various regions across the bone, which indicated that tendon-periosteum-like tissues lie in the CT-density range of GSR. Furthermore, parts of the ear cartilages, thin facial skeletal bones and ocular lenses became visible in the GSR-typical density range. As these were not considered in the pragmatic build of the statistical model as consequence of practical consideration, this was expected.

Discussion

We approached a fast and rapid visualization of presumed GSR in PMCT based on prior research, which had clearly shown that it is possible to do this, and that had shown that in 3-dimensional visualization, particular shapes may result [1]. With that, existing emphasis of regular PMCT on solid metal density in gunshot victim examination [8–12] may be expanded towards lower densities. Even micro-CT based research fo GSR so far only focused on visualization in the high CT-density range [13].

We implemented this in two softwares, one commercial and one free. Our method as outlined in this technical note can easily be implemented also in other free softwares, such as Horos[7], Osirix[8], or 3D-Slicer[9].

Visualizing presumed GSR in routine PMCT may be tedious if performed individually, on a case-by-case basis and manually, so a preset

Table 1
Tabular listing of presumedly GSR-typical shapes identified in PMCT.

Case	Presumed GSR visualization in vicinity of head gunshot wound	False positive: presumed anatomical correlates
1	Entrance wound: Semicircular arrangement of coalescing little blebs, around 30 mm in diameter.	Ear cartilage parts, ocular lenses and periosteum.
2	Entrance wound: Ring shaped structure, around 25 mm in diameter.	Post mortem decomposition; in that context, unanimous attribution to anatomical structures seems out of reach.
3	Entrance wound: Relatively flat structure with a central defect, around 27 mm in diameter.	Ear cartilage parts, ocular lenses and periosteum.
4	Entrance wound: Scattered blebs, partly in semicircular or ring-shaped arrangement, diameter of around 18 mm.	Cartilage, ocular lenses and periosteum.
5	Entrance wound: Circumferential scattered deposits.	Cartilage, ocular lenses and periosteum.
6	Entrance wound: Circumferential mostly scattered, partly coalesced deposits.	Cartilage, ocular lenses and periosteum.
7	Entrance wound: Ring-shaped arrangement of little blebs surrounding entrance wound, also GSR-typical density of attached blood clot.	Cartilage, ocular lenses, aponeurotic tissue and tendons, and periosteum.
3	Exit wound: Negative.	See above.
4	Exit wound: Negative.	See above.

[7] Horos, Bernex, Switzerland, https://horosproject.org/
[8] Pixmeo SARL, Bernex, Switzerland, https://www.osirix-viewer.com/
[9] Harvard University and Isomics Inc., Cambridge, Massachusetts, USA, https://www.slicer.org/

based solution was developed. Technically, Bayesian likelihood ratios based on data probabilities are known to work for 3D-visualization [7], and they can be also based on assumptions and simplification. Using normal distributions based on measured CT-density data from regions of interest measurements constitutes a simplification; instead, actual distributions could be determined with more extensive efforts, and more sophisticated distribution functions could be used [14]. In terms of tissue categories, we used focused categorial measurements as basis for estimating the most likely GSR-typical density range, rather than very finely tuned tissue and material density measurements. There, bone fragments, compressed or burned tissue, as well as burned blood may well have to be considered particularly in context of analysing gunshot wounds. This might be improved, however, only with a possibly significant extra effort at possibly small gains [5].

In this study, resulting density values used for the 3D-visualization presets and reconstructed images, however, plausibly match visual evidence, shape patterns that are documented elsewhere in both CT- and micro-CT based GSR studies and were negative also when checked in exit wounds in two instances in our case series. As this technical note for a visualization approach does not attempt completeness, further research may have to identify the appearances of different types of injuries in the light of such new visualizations.

The localizations and shapes of GSR-typical visualizations indicate already from our case series, that GSR as product of a highly dynamical process seems to remain a dynamically influenced phenomenon after the shot was fired: other processes, such as ante- or peri-mortal hemorrhage, may displace GSR as illustrated in one case (Case 7) where a blood clot appeared to contain presumed GSR particles in a somewhat dissolved or dispersed state and apparently displaced some of that material.

GSR as a material may be described as a finely dispersed collection of metal particles. While these may be identified as particles in micro-CT both in terms of particle-like shape and by high density typical for solid metal, they tend to succumb to partial volume effect in less highly resolved scanners and thus may lose their apparently metal-specific high density. This is likely to happen despite exploiting the maximal resolution of a clinical whole body CT scanner as used in most forensic routine settings [15]. That is why in routine CT, it is plausible that GSR as locally condensed metal particles may be identified at densities such as the identified range between 87 and 105 HU rather than at densities typical for solid metals, which tend to be far in excess of 1000 HU. As presumed GSR may appear also as compressed rather than dispersed metal particles, the assumption of partial volume effect is not always met, presulting in GSR visualizations with higher CT-densities such as in case 4 (Fig. 5). And yet, we may be just looking at a part of a variably aggregated particle scatter whose true extent may exceed even the capabilities of an average micro-CT [16].

A clear limitation of our PMCT visualization study is that we did not perform any further validation of the presumed GSR presence other than visual identification. No proof of GSR was sought, and presumed GSR was identified only by plausibilization based on written and photographic documentation, and based on prior research that documented, e.g., shapes such as blebs, scattered deposits, rings and cones, with a delineation, location and relative morphology in relation to the visual findings of the body, that we regarded as typical for entrance wound GSR. Conversely, routine imaging appears to be a great screening tool before investigating possible presence of GSR with more precise and expensive methods. Once a fast and plausible visualization is achieved, possible presence of GSR may be routinely reported [17–19] to the forensic pathologist on a larger scale of cases, and a more focused follow-up based on prior evidence may be targeted more economically.

Another limitation of this method is a reduced selection of tissues that were selected to make presumed GSR stand out visually, particularly, omitting also cartilage and periosteum. A simplified statistical model assuming normal distributions was chosen when a non-parametric and more expensive approach might give better results.

Clearly, more research is required to establish better criteria for GSR visualization. The search for GSR may need to be performed on a wider basis. It may also need to be investigated what shapes and distribution patterns GSR can assume in context of real wound morphology of terminal ballistics to gain a better understanding. Future studies may also focus on using dual energy to better separate cartilage from GSR and on the use of micro-CT to confirm the distribution of GSR in tissue blocks.

Ethical approval

Data usage for this study is conformant with Swiss laws and ethical standards as approved by the Ethics Committee of the Canton of Zurich (written approval, KEK ZH-Nr. 15-0686).

Declaration of Competing Interest

The authors declare that they have no known competing financial interests or personal relationships that could have appeared to influence the work reported in this paper.

Acknowledgements

The authors express their gratitude to Emma Louise Kessler, MD for her generous donation to the Zurich Institute of Forensic Medicine, University of Zurich, Switzerland.

References

[1] K. Stein, M. Bahner, J. Merkel, S. Ain, R. Mattern, Detection of gunshot residues in routine cts, Int. J. Legal Med. 114 (1-2) (2000) 15–18.
[2] L.C. Ebert, W. Schweitzer, D. Gascho, T.D. Ruder, P.M. Flach, M.J. Thali, G. Ampanozi, Forensic 3d visualization of ct data using cinematic volume rendering: a preliminary study, Am. J. Roentgenol. 208 (2) (2017) 233–240.
[3] F. Berger, L.C. Ebert, R.A. Kubik-Huch, K. Eid, M.J. Thali, T. Niemann, Application of cinematic rendering in clinical routine ct examination of ankle sprains, Am. J. Roentgenol. (2018) 1–4.
[4] P.M. Flach, D. Gascho, W. Schweitzer, T.D. Ruder, N. Berger, S.G. Ross, M.J. Thali, G. Ampanozi, Imaging in forensic radiology: an illustrated guide for postmortem computed tomography technique and protocols, Forens. Sci. Med. Pathol. 10 (4) (2014) 583–606.
[5] J.O. Berger, B. Liseo, R.L. Wolpert, et al., Integrated likelihood methods for eliminating nuisance parameters, Stat. Sci. 14 (1) (1999) 1–28.
[6] T. Karlsson, Multivariate analysis (forensiometrics)–a new tool in forensic medicine. differentiation between firearm-related homicides and suicides, Forens. Sci. Int. 101 (2) (1999) 131–140.
[7] J.M. Kniss, R. Van Uitert, A. Stephens, G.-S. Li, T. Tasdizen, C. Hansen, Statistically quantitative volume visualization. IEEE Visualization 2005, IEEE, Minneapolis, MN, USA, 2005, pp. 287–294.
[8] M.J. Thali, K. Yen, P. Vock, C. Ozdoba, B.P. Kneubuehl, M. Sonnenschein, R. Dirnhofer, Image-guided virtual autopsy findings of gunshot victims performed with multi-slice computed tomography (msct) and magnetic resonance imaging (mri) and subsequent correlation between radiology and autopsy findings, Forens. Sci. Int. 138 (1-3) (2003) 8–16.
[9] G. Ampanozi, N. Schwendener, A. Krauskopf, M.J. Thali, C. Bartsch, Incidental occult gunshot wound detected by postmortem computed tomography, Forens. Sci. Med. Pathol. 9 (1) (2013) 68–72.
[10] P.M. Flach, G. Ampanozi, T. Germerott, S.G. Ross, A. Krauskopf, M.J. Thali, M. T. Mund, Shot sequence detection aided by postmortem computed tomography in a case of homicide, J. Forens. Radiol. Imag. 1 (2) (2013) 68–72.
[11] G. Ampanozi, T. Ruder, L. Ebert, M. Thali, P. Flach, Gunshots to the head: characteristics on post-mortem ct, J. Forens. Radiol. Imag. 1 (2) (2013) 77.
[12] S.A. Bolliger, G. Ampanozi, B.P. Kneubuehl, M.J. Thali, Gunshot to the pelvis–experimental ballistics and forensic radiology, J. Forens. Radiol. Imag. 2 (1) (2014) 17–19.
[13] G. Cecchetto, C. Giraudo, A. Amagliani, G. Viel, P. Fais, F. Cavarzeran, G. Feltrin, S. D. Ferrara, M. Montisci, Estimation of the firing distance through micro-ct analysis of gunshot wounds, Int. J. Legal Med. 125 (2) (2011) 245–251.
[14] G.H. John, P. Langley, Estimating continuous distributions in bayesian classifiers. Proceedings of the Eleventh conference on Uncertainty in artificial intelligence, Morgan Kaufmann Publishers Inc., 1995, pp. 338–345.
[15] J.M. Ford, S.J. Decker, Computed tomography slice thickness and its effects on three-dimensional reconstruction of anatomical structures, J. Forens. Radiol. Imag. 4 (2016) 43–46.
[16] G. Rutty, A. Brough, M. Biggs, C. Robinson, S. Lawes, S. Hainsworth, The role of micro-computed tomography in forensic investigations, Forens. Sci. Int. 225 (1-3) (2013) 60–66.
[17] G. Ampanozi, D. Zimmermann, G.M. Hatch, T.D. Ruder, S. Ross, P.M. Flach, M. J. Thali, L.C. Ebert, Format preferences of district attorneys for post-mortem

medical imaging reports: understandability, cost effectiveness, and suitability for the courtroom: a questionnaire based study, Legal Med. 14 (3) (2012) 116–120.

[18] B. Morgan, A. Alminyah, A. Cala, C. O'Donnell, D. Elliott, G. Gorincour, P. Hofman, M. Iino, Y. Makino, A. Moskata, et al., Use of post-mortem computed tomography in disaster victim identification. positional statement of the members of the disaster victim identification working group of the international society of forensic radiology and imaging; may 2014, J. Forens. Radiol. Imag. 2 (3) (2014) 114–116.

[19] W. Schweitzer, C. Bartsch, T.D. Ruder, M.J. Thali, Virtopsy approach: structured reporting versus free reporting for pmct findings, J. Forens. Radiol. Imag. 2 (1) (2014) 28–33.